AIMS Energy, 13(5): 1320–1346.
DOI: 10.3934/energy.2025049
Received: 27 June 2025
Revised: 04 September 2025
Accepted: 17 September 2025
Published: 20 October 2025

https://www.aimspress.com/journal/energy

Research article

Optimal operation of integrated energy system considering source load uncertainty and equipment capacity optimization

Ruoli Tang, Chao Jiang*, Xin Li, Yinchen Zhang, Zelong Li and Mingyue Xu

School of Naval Architecture, Ocean and Energy Power Engineering, Wuhan University of Technology, Wuhan, Hubei, China

* **Correspondence:** Email: 345509@whut.edu.cn. Tel: +18716762422.

Abstract: Due to the increasingly stringent environmental protection policies, the integrated energy system (IES) plays a vital role in improving energy efficiency and reducing carbon emissions (CE). To achieve optimal operation of IES, a method that considers source load uncertainty and equipment capacity optimization is proposed in this study. First, an IES model including electricity, heat, and gas energies is established, and a ladder-type carbon trading mechanism model is introduced to implement CE restrictions. Furthermore, by considering the horizontal transfer and vertical complementary substitution of electricity, heat, and gas loads, an integrated demand response (IDR) model is proposed. Second, in order to achieve the minimization of the IES comprehensive cost, the equipment capacity optimization is introduced into the developed operation model. Then, the optimal operation model is established and transformed into a constrained mixed integer linear problem, which can be directly solved by the commercial solver CPLEX. Finally, the information gap decision theory is used for solving the source load uncertainty problem, and a risk-averse robust model is proposed. Experimental results showed that when IDR is considered, the total operating (TO) cost is reduced from 29130.69 to 27470.67 CNY (5.70% reduction), and CE is reduced from 28788.92 to 25391.62 kg (11.80% reduction). Moreover, by introducing the equipment capacity optimization, the TO cost is further reduced from 27470.67 to 27071.28 CNY (1.45% reduction), and CE is further reduced from 25391.62 to 25114.43 kg (1.09% reduction). Simultaneously, when the source load uncertainty is considered, the TO cost is increased from 27071.28 to 28424.85 CNY (5.00% increase), and CE is increased from 25114.43 to 27560.31 kg (9.74% increase). However, the risk-bearing ability can be significantly improved, and the operational stability is also increased.

Keywords: integrated energy system; integrated demand response; optimal operation; equipment capacity optimization; source load uncertainty

Abbreviations: IES: Integrated energy system; CE: Carbon emission; IDR: Integrated demand response; TO: Total operating; SLU: Source load uncertainty; EC: Equipment capacity; IGDT: Information gap decision theory; PG: Power grid; GG: Gas grid; WT: Wind turbine; PV: Photovoltaic; P2G: Power to gas; CHP: Combined heating and power; GB: Gas-fired boiler; EES: Electrical energy storage; HES: Heat energy storage; GES: Gas energy storage; GT: Gas turbine; WHB: Waste heat boiler; CT: Carbon trading; EP: Energy purchase; EM: Equipment maintenance; DEEI: Daily equivalent of equipment investment; EPP: Electricity power purchase; WTPPAP: Wind turbine and photovoltaic power abandonment penalty; GPP: Gas power purchase

1. Introduction

Energy consumption is a common concern in today's society. With increasingly serious problems such as a shortage of fossil energy, environmental deterioration, and climate warming, promoting energy transformation and the use of renewable energy technology is important to cope with these problems [1,2]. The integrated energy system (IES), as a new energy supply method, achieves optimal allocation and efficient utilization of energy by tightly coupling the production, transmission, storage, and consumption of various energies. The IES integrates multiple energy forms, such as electricity, heat, and gas, which significantly enhances energy utilization efficiency, reduces carbon emissions (CE), and promotes green transformation of energy structure through intelligent management and coordinated optimization [3,4].

Numerous scholars have conducted extensive research on the optimal operation of IES. Zhang et al. proposed a low-carbon economic model of IES by optimally dispatching electricity and heat flows and adjusting the output of each unit. Experimental results showed that their method significantly enhanced the consumption of renewable energy and reduced the CE [5]. Dong et al. proposed an operation method of IES, which considered the hybrid structure of electrical and heat energy storage. With the application of their method, the coupling of various energies was effectively optimized, and the energy utilization efficiency was also improved [6]. Zhang et al. proposed a multi-objective optimization method of operation strategies in the IES, in which the integrated demand response (IDR) and dynamic pricing were considered. With their developed method, the economy and reliability of IES operation were improved, and the interaction among different stakeholders was also facilitated [7]. Ding et al. considered IDR and established a comprehensive energy efficiency model of IES. They also developed a multi-objective optimization method in order to maximize comprehensive energy efficiency and minimize the operating cost [8]. Wang et al. also considered the IDR as an important measure for the optimal operation of IES. In their study, a multi-objective optimization method was established, which significantly enhanced the economic and efficient operation of IES [9]. Xiang et al. primarily explored the economic and environmental benefits of IDR, which significantly improved energy utilization rates of the IES [10,11]. Zhou et al. proposed a hybrid hydrogen-battery compensation operation with a transient aging model, which provided frontier guidelines for the design, operation, and carbon-neutral transformation of multi-energy systems [12]. Zhang et al. proposed an integrated fuel cell electric vehicle-building cogeneration framework with

optimized configurations and synergistic control strategies, which enhanced energy flexibility and techno-economic and environmental performance and mitigated fuel cell degradation in subtropical buildings [13]. Yang et al. proposed a co-optimization model with ladder-type CT mechanism and multi-energy IDR, which reduced the TO cost and CE of IES [14]. Liu et al. proposed an IES optimal dispatch model considering IDR and evaluated the performance in terms of economy, reliability, and environment [15]. As discussed above, most existing studies often overlooked the source load uncertainty (SLU) problem. Moreover, the impact of equipment capacity (EC) optimization is also rarely considered in the operation of IES. Therefore, most of the existing methods cannot be directly used in real-world applications if the impact of the SLU problem and EC optimization cannot be ignored.

In addition, there are three kinds of methods that can be used to solve the SLU problem: fuzzy optimization, stochastic optimization, and robust optimization. Li et al. defined the wind speed as a random fuzzy variable and established a stochastic fuzzy chance constrained optimization method. However, the fuzzy optimization is often highly subjective [16]. Mei et al. proposed a distributed IES stochastic optimization operation method based on multiple scenario simulations, in which the predictive uncertainties of renewable energy and loads were considered. According to the experimental results, the operational safety was ensured, and the consumption of renewable energy was also enhanced. However, stochastic optimization is overly reliant on the probabilistic models of uncertainties [17]. Sun et al. proposed a two-stage robust optimization method by considering the safety margin, and the power supply reliability of IES was improved. However, robust optimization tends to consider the worst scenarios, often leading to overly conservative results [18]. Compared with the aforementioned methods, the information gap decision theory (IGDT) is a non-probabilistic and non-fuzzy method, which could effectively quantify uncertainty when some of the information is unknown [19]. Sun et al. proposed a novel integrated stochastic optimization IGDT method to solve the multiple uncertainties of IES and optimize its operation plan [20]. Wang et al. proposed a multi-objective operational optimization method based on IGDT, in which the capacities of mixed energy storage were planned to cope with multiple uncertainties. In addition, the daily operational profits could be maximized [21]. Jordehi et al. established an IES operation method in which the loads and electricity price uncertainties were considered [22]. Peng et al. introduced an optimization method based on IGDT to solve the issues of strong subjectivity and insufficient robustness in previous energy storage configuration methods. With the developed method, the comprehensive benefit of the energy storage system was significantly enhanced [23].

In this study, a novel operation method for the IES under complex conditions is developed, in which the IDR, SLU problem, and EC optimization are considered. With this method, the economic and environmental performance of the system can be improved while the operational stability is also ensured. First, the IDR model is established by considering the horizontal transfer and vertical complementary substitution of loads. Second, in order to minimize the TO cost of IES, a collaborative optimization method of supply and demand side resources is developed. Third, based on the IGDT, a robust model under a risk-averse strategy is established to solve the SLU problem. Finally, the effectiveness of the proposed method is verified by a comparative set of scenario analyses.

2. Structure and operation model of the integrated energy system

The IES can facilitate the comprehensive utilization of multiple energies. The structure of IES proposed in this study is shown in Figure 1, in which the electricity, heat, and gas loads of users are

considered. As shown in Figure 1, the system is divided into the energy supply side, energy hub side, and energy demand side. The energy supply side includes the power grid (PG), gas grid (GG), wind turbine (WT), and photovoltaic (PV) system; the energy hub side includes the power to gas (P2G), combined heating and power (CHP), gas-fired boiler (GB), electrical energy storage (EES), heat energy storage (HES), and gas energy storage (GES). Among them, the CHP consists of the gas turbine (GT) and waste heat boiler (WHB). The energy demand side includes electricity, heat, and gas loads. The electricity load is satisfied by the PG, WT, PV, CHP, and EES; the heat load is satisfied by the CHP, GB, and HES; the gas load is satisfied by the GG, P2G, and GES.

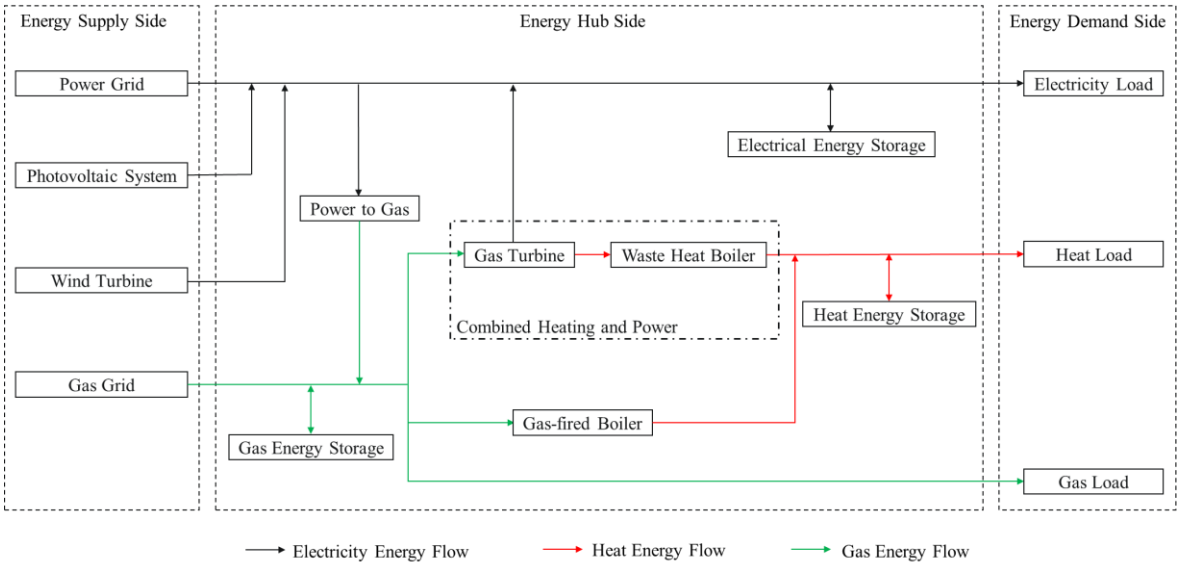

Figure 1. Structure of the IES.

2.1. Equipment models

2.1.1. Power-to-gas model

The P2G is an energy conversion equipment that electrolyzes water to produce hydrogen and then reacts chemically with carbon dioxide from the air to produce natural gas. The operation model of the P2G can be formulated as [24]:

$$P_{P2G,g}(t) = \eta_{P2G,g} P_{P2G,e}(t) \tag{1}$$

where $P_{P2G,g}(t)$ represents the natural gas power output during time period t; $\eta_{P2G,g}$ represents the energy conversion efficiency; and $P_{P2G,e}(t)$ represents the electricity power input during time period t.

2.1.2. Combined heating and power model

The CHP consists of the GT and WHB. The GT generates electricity by combusting natural gas, and the discharged waste heat is captured by the WHB for heat supply. The operation model of CHP can be formulated as [25]:

$$P_{CHP,e}(t) = \eta_{GT,e} L_{NG} G_{CHP,g}(t) \tag{2}$$

$$H_{GT}(t) = \left(1 - \eta_{GT,e} - \eta_{GT,loss}\right) G_{CHP,g}(t) L_{NG} \tag{3}$$

$$P_{CHP,h} = \eta_{WHB,h} H_{GT}(t) \tag{4}$$

where $P_{CHP,e}(t)$ represents the electricity power output during time period t; $\eta_{GT,e}$ represents the power generation efficiency; L_{NG} represents the lower heating value of natural gas; $G_{CHP,g}(t)$ represents the volume of natural gas consumed during time period t, in cubic meters; $H_{GT}(t)$ represents the discharged waste heat power output during time period t; $\eta_{GT,loss}$ represents the heat loss rate; $P_{CHP,h}(t)$ represents the heat power output during time period t; and $\eta_{WHB,h}$ represents the energy conversion efficiency.

2.1.3. Gas-fired boiler model

The GB transforms chemical energy into heat energy by burning natural gas to satisfy the heat demands of users. The operation model of GB can be formulated as [26]:

$$P_{GB,h}(t) = \eta_{GB,h} L_{NG} G_{GB,g}(t) \tag{5}$$

where $P_{GB,h}(t)$ represents the heat power output during time period t; $\eta_{GB,h}$ represents the heating efficiency; and $G_{GB,g}(t)$ represents the volume of natural gas consumed during time period t in cubic meters.

2.1.4. Energy storage model

The energy storage operation characteristics can be described by capacity, charging/discharging power, and efficiency. The EES, HES, and GES can be expressed through a unified operation model [27]:

$$W_i(t+1) = \left(1 - \sigma_i\right) W_i(t) + \left(\eta_{i,c} P_{i,c}(t) - \frac{P_{i,d}(t)}{\eta_{i,d}}\right) \Delta t \tag{6}$$

where i represents the type of energy storage equipment (including EES, HES, and GES); σ_i represents the self-loss coefficient of energy storage equipment i; $W_i(t)$ represents the capacity of energy storage equipment i during time period t; $\eta_{i,c}$ and $\eta_{i,d}$ represent the charging and discharging efficiencies of energy storage equipment i, respectively; $P_{i,c}(t)$ and $P_{i,d}(t)$ represent the charging and discharging power of energy storage equipment i during time period t, respectively; and Δt represents the time interval.

2.2. Ladder-type carbon trading mechanism model

The carbon trading market is currently gaining popularity; a well-established carbon trading market can promote CE reduction across various industries to a certain extent. Regulatory authorities issue the free CE quota to the IES. When the CE generated by the IES is below the allocated quota,

the surpluses can be sold in the carbon trading market. On the contrary, the excess portion must be purchased if the quota is exceeded. The aforementioned carbon trading mechanism mainly consists of three components: the initial CE quota, actual CE, and carbon trading (CT) cost [28].

2.2.1. Initial carbon emission quota model

The current quota method primarily adopts a gratuitous distribution [29]. The main CE sources within the IES include the coal-fired power units, CHP, GB, and gas load. The initial quota model can be formulated as:

$$\begin{cases} E_{IES} = E_{E,buy} + E_{CHP} + E_{GB} + E_{G,load} \\ E_{E,buy} = \alpha_E \sum_{t=1}^{T} P_{E,buy}(t) \\ E_{CHP} = \alpha_H \sum_{t=1}^{T} (\alpha_{E,h} P_{CHP,e}(t) + P_{CHP,h}(t)) \\ E_{GB} = \alpha_H \sum_{t=1}^{T} P_{GB,h}(t) \\ E_{G,load} = \alpha_{G,load} \sum_{t=1}^{T} P_{G,load}(t) \end{cases} \tag{7}$$

where E_{IES} represents the CE quota of IES; $E_{E,buy}$ represents the CE quota of electricity power purchased from PG; E_{CHP}, E_{GB}, and $E_{G,load}$ represent the CE quota of CHP, GB, and gas load, respectively; α_E, α_H, and $\alpha_{G,load}$ represent the CE quota of generating a unit of electricity power, a unit of heat power, and consuming a unit of gas load, respectively; $\alpha_{E,h}$ represents the conversion coefficient of electricity and heat power; $P_{E,buy}(t)$ represents the electricity power purchased from PG during time period t; $P_{G,load}(t)$ represents the gas load demand during time period t; and T represents the operation cycle.

2.2.2. Actual carbon emission model

It is assumed that all electricity power purchased from the PG is derived from coal-fired power units. The gas load is primarily consumed through combustion, which also generates CE. In addition, the P2G can absorb a portion of CE during its operation. If the P2G operation process is considered, the initial CE model needs to be revised. Consequently, the actual CE model can be expressed as:

$$\begin{cases} E_{IES,a} = E_{E,buy,a} + E_{CHPGB,a} + E_{G,load,a} - E_{P2G,a} \\ E_{E,buy,a} = \sum_{t=1}^{T} (x_1 + y_1 P_{E,buy}(t) + z_1 P_{E,buy}^2(t)) \\ E_{CHPGB,a} = \sum_{t=1}^{T} (x_2 + y_2 P_{CHPGB}(t) + z_2 P_{CHPGB}^2(t)) \\ P_{CHPGB}(t) = P_{CHP,e}(t) + P_{CHP,h}(t) + P_{GB,h}(t) \\ E_{G,load,a} = \sum_{t=1}^{T} \beta P_{G,load}(t) \\ E_{P2G,a} = \sum_{t=1}^{T} \gamma P_{P2G,g}(t) \end{cases} \tag{8}$$

where $E_{IES,a}$ represents the actual CE of IES; $E_{E,buy,a}$ represents the actual CE of electricity power purchased from the PG; $E_{CHPGB,a}$ represents the total actual CE of CHP and GB; $E_{G,load,a}$ represents the actual CE of gas load; $E_{P2G,a}$ represents the actual CE absorption during the P2G operation process; $P_{CHPGB}(t)$ represents the equivalent output power of CHP and GB during time period t; x_1, y_1, and z_1 are the CE calculation coefficients of coal-fired power units; x_2, y_2, and z_2 are the CE calculation coefficients of natural gas-fired units; β is the equivalent CE coefficient per unit of the gas load; and γ is the coefficient of CE absorption during the P2G operation process.

2.2.3. Carbon trading model

Once the CE quota and actual CE of IES are determined, the CE trading amount that participates in the carbon trading market can be calculated as:

$$E_{IES,b} = E_{IES,a} - E_{IES} \tag{9}$$

where $E_{IES,b}$ represents the CE trading amount of IES.

The ladder-type carbon trading mechanism divides multiple CE purchase intervals, and the purchase price increases with the quota that the IES needs to purchase. The ladder-type carbon trading model can be expressed as:

$$C_{CO_2} = \begin{cases} \lambda E_{IES,b}, & E_{IES,b} \le d \\ \lambda(1+\delta)(E_{IES,b} - d) + \lambda d, & d < E_{IES,b} \le 2d \\ \lambda(1+2\delta)(E_{IES,b} - 2d) + (2+\delta)\lambda d, & 2\mathrm{d} < E_{IES,b} \le 3d \\ \lambda(1+3\delta)(E_{IES,b} - 3d) + (3+3\delta)\lambda d, & 3d < E_{IES,b} \le 4d \\ \lambda(1+4\delta)(E_{IES,b} - 4d) + (4+6\delta)\lambda d, & 4d < E_{IES,b} \le 5d \\ \lambda(1+5\delta)(E_{IES,b} - 5d) + (5+10\delta)\lambda d, & 5d < E_{IES,b} \end{cases} \tag{10}$$

where C_{CO_2} represents the CT cost; λ represents the base price of carbon trading; d represents the length of the CE amount interval; and δ represents the increase rate of price.

2.3. Integrated demand response model

Furthermore, the IDR model is proposed by considering horizontal transfer and vertical complementary substitution of electricity, heat, and gas loads.

According to different price signals, the horizontal transfer of loads refers to loads transferring in the energy consumption time, while vertical complementary substitution means that users can choose different forms of energy supply to achieve the same goal. As the electricity, heat, and gas loads all have the capabilities of horizontal transfer and vertical complementary substitution, they can be divided into three parts: the fixed load, transferable load, and substitutable load, which can be expressed as [30]:

$$P_{K,load}(t) = P_{K,load}^{f,0}(t) + P_{K,load}^{t,0}(t) + P_{K,load}^{s,0}(t) \tag{11}$$

where $K \in \{E, H, G\}$ represents the load type, including electricity, heat, and gas loads, respectively; $P_{K,load}(t)$ represents the value of load K during time period t; $P_{K,load}^{f,0}(t)$ represents the initial fixed value of load K during time period t; $P_{K,load}^{t,0}(t)$ represents the initial transferable value of load K during time period t; and $P_{K,load}^{s,0}(t)$ represents the initial substitutable value of load K during time period t.

The detailed models of fixed load, transferable load, and substitutable load are established as follows:

1) The fixed loads of electricity, heat, and gas do not participate in IDR.

2) The transferable loads can be transferred in the time dimension during the operation cycle, which can be expressed as:

$$\begin{cases} P_{K,load}^{t}(t) = P_{K,load}^{t,0}(t) + \Delta P_{K,load}^{t}(t) \\ \Delta P_{K,load}^{t}(t) = A_K^{t,in}(t) P_{K,load}^{t,in}(t) - A_K^{t,out}(t) P_{K,load}^{t,out}(t) \\ A_K^{t,in}(t) + A_K^{t,out}(t) \le 1 \\ \sum_{t=1}^{T} \Delta P_{K,load}^{t}(t) = 0 \\ \varepsilon_{K,\min}^{t} P_{K,load}^{t,0}(t) \le \Delta P_{K,load}^{t}(t) \le \varepsilon_{K,\max}^{t} P_{K,load}^{t,0}(t) \end{cases} \tag{12}$$

where $P_{K,load}^{t}(t)$ represents the value of transferable load K during time period t after the horizontal transfer; $\Delta P_{K,load}^{t}(t)$ represents the variation of $P_{K,load}^{t,0}(t)$ in the horizontal transfer; $A_K^{t,in}(t)$ and $A_K^{t,out}(t)$ are binary variables, which represent the transfer-in and transfer-out parameters of transferable load K during time period t, respectively; $P_{K,load}^{t,in}(t)$ and $P_{K,load}^{t,out}(t)$ represent the transfer-in and transfer-out power of transferable load K during time period t, respectively; and $\varepsilon_{K,\min}^{t}$ and $\varepsilon_{K,\max}^{t}$ represent the upper and lower limit proportions of transferable load K during each period, respectively, which are used to ensure the quality of energy demand for the users. Note that the fourth sub-equation of Eq (12) shows that the total amount of transferable load K should remain unchanged over an operation cycle.

3) The substitutable load: Users can choose a different energy supply to satisfy their demands within the same time period. This can be reflected in the following specific life examples:

① For hot water demands, users can choose to use the heat power supplied by the IES or choose to use electricity or gas water heaters.

② For heating demands, users can also choose to use the heat power supplied by the IES or choose electric air conditioner.

③ For cooking demands, users can choose to use electromagnetic cookstoves or gas cookstoves.

The vertical complementary substitution of loads does not change the users' energy demands, thus it does not impact them. This flexibility allows for a more efficient and potentially cost-effective use of energy resources while maintaining the quality of service for the users.

$$\begin{cases} P_{K,load}^{s}(t) = P_{K,load}^{s,0}(t) + \Delta P_{K,load}^{s}(t) \\ \Delta P_{K,load}^{s}(t) = A_{K}^{s,in}(t) P_{K,load}^{s,in}(t) - A_{K}^{s,out}(t) P_{K,load}^{s,out}(t) \\ A_{K}^{s,in}(t) + A_{K}^{s,out}(t) \le 1 \\ \sum\limits_{K \in \{E,H,G\}} P_{K,load}^{s}(t) = 0 \\ \varepsilon_{K,\min}^{s} P_{K,load}^{s,0}(t) \le \Delta P_{K,load}^{s}(t) \le \varepsilon_{K,\max}^{s} P_{K,load}^{s,0}(t) \end{cases} \tag{13}$$

where $P_{K,load}^{s}(t)$ represents the value of substitutable load K during time period t after the vertical complementary substitution; $\Delta P_{K,load}^{s}(t)$ represents the variation of $P_{K,load}^{s,0}(t)$ in the vertical complementary substitution; $A_{K}^{s,in}(t)$ and $A_{K}^{s,out}(t)$ are binary variables, which represent the substituting and replaced parameters of substitutable load K during time period t, respectively; $P_{K,load}^{s,in}(t)$ and $P_{K,load}^{s,out}(t)$ represent the substituting and replaced power of substitutable load K during time period t, respectively; and $\varepsilon_{K,\min}^{s}$ and $\varepsilon_{K,\max}^{s}$ represent the upper and lower limit proportions of substitutable load K during each period, respectively, which are also used to ensure the quality of energy demand for the users. Note that the fourth sub-equation of Eq (13) shows that the sum of all substitutable loads should equal 0 during the time period.

3. Integrated energy system operation model and solution method

3.1. Objective function

The method proposed in this study takes 24 h as the operation cycle and comprehensively considers the energy purchase (EP) cost C_{BUY}, equipment maintenance (EM) cost C_{OPE}, and CT cost C_{CO_2}, daily equivalent of equipment investment (DEEI) cost C_{INV}, as well as wind turbine and photovoltaic power abandonment penalty (WTPPAP) cost C_{DG}. The objective function of IES can be established as:

$$\min C = C_{BUY} + C_{OPE} + C_{CO_2} + C_{INV} + C_{DG} \tag{14}$$

1) EP cost

The EP cost of IES includes the electricity power purchase (EPP) cost and gas power purchase (GPP) cost, which can be formulated as:

$$C_{BUY} = \sum_{t=1}^{T} \psi(t) P_{E,buy}(t) + \sum_{t=1}^{T} \varphi(t) P_{G,buy}(t) \tag{15}$$

where $P_{G,buy}(t)$ represents the gas power purchased from GG during the time period t; and $\psi(t)$ and $\varphi(t)$ represent the electricity price and natural gas price during time period t, respectively.

2) EM cost

The calculation of EM cost is as follows:

$$C_{OPE} = \sum_{t=1}^{T}\sum_{j=1}^{N_M} C_{M,j}\left|P_j(t)\right| \tag{16}$$

where N_M represents the total number of equipment within the IES; $C_{M,j}$ represents the unit maintenance cost of equipment j; and $P_j(t)$ represents the output power of equipment j during time period t.

3) CT cost

The calculation of CT cost is detailed in Eq (10).

4) DEEI cost

The calculation of DEEI cost is as follows:

$$C_{INV} = \sum_{j} \frac{C_j W_j}{365} \frac{r(1+r)^{N_j}}{(1+r)^{N_j}-1} \tag{17}$$

where C_j represents the unit capacity investment cost of equipment j; W_j represents the capacity to be configured of equipment j; N_j represents the service life of equipment j; and r represents the discount rate.

5) WTPPAP cost

The calculation of WTPPAP cost is as follows:

$$C_{DG} = \sum_{t=1}^{T} \chi_{DG}(P_{WT,cut}(t) + P_{PV,cut}(t)) \tag{18}$$

where χ_{DG} represents the penalty cost per unit of WT and PV power abandonment; and $P_{WT,cut}(t)$ and $P_{PV,cut}(t)$ represent WT and PV power abandonment during time period t, respectively.

3.2. Constraints

1) WT power output constraint

$$0 \le P_{WT}(t) \le \eta_{WT} W_{WT} \tag{19}$$

$$0 \le W_{WT} \le W_{WT,0} \tag{20}$$

where $P_{WT}(t)$ represents the WT power during time period t; η_{WT} represents the predicted output factor of WT, which is set within the interval [0, 1]; W_{WT} represents the capacity of WT; and $W_{WT,0}$ represents the initial capacity of WT.

2) PV power output constraint

$$0 \le P_{PV}(t) \le \eta_{PV} W_{PV} \tag{21}$$

$$0 \le W_{PV} \le W_{PV,0} \tag{22}$$

where $P_{PV}(t)$ represents the output power of the PV system during time period t; η_{PV} represents the predicted output factor of the PV system, which is set within the interval [0, 1]; W_{PV} represents the capacity of the PV system; and $W_{PV,0}$ represents the initial capacity of PV.

3) CHP operation constraint

$$\begin{cases} 0 \le P_{CHP,e}(t) \le W_{CHP} \\ \kappa_{CHP,e}^{down} W_{CHP} \le P_{CHP,e}(t) - P_{CHP,e}(t-1) \le \kappa_{CHP,e}^{up} W_{CHP} \end{cases} \tag{23}$$

$$0 \le W_{CHP} \le W_{CHP,0} \tag{24}$$

where W_{CHP} represents the capacity of CHP; $\kappa_{CHP,e}^{down}$ and $\kappa_{CHP,e}^{up}$ represent the ramp-up and ramp-down limits of CHP, respectively; $W_{CHP,0}$ represents the initial capacity of CHP.

4) GB operation constraint

$$\begin{cases} 0 \le P_{GB,h}(t) \le W_{GB} \\ \kappa_{GB,h}^{down} W_{GB} \le P_{GB,h}(t) - P_{GB,h}(t-1) \le \kappa_{GB,h}^{up} W_{GB} \end{cases} \tag{25}$$

$$0 \le W_{GB} \le W_{GB,0} \tag{26}$$

where W_{GB} represents the capacity of GB; $\kappa_{GB,h}^{down}$ and $\kappa_{GB,h}^{up}$ represent the ramp-up and ramp-down limits of GB, respectively; and $W_{GB,0}$ represents the initial capacity of GB.

5) P2G operation constraint

$$\begin{cases} 0 \le P_{P2G,g}(t) \le W_{P2G} \\ \kappa_{P2G,g}^{down} W_{P2G} \le P_{P2G,g}(t) - P_{P2G,g}(t-1) \le \kappa_{P2G,g}^{up} W_{P2G} \end{cases} \tag{27}$$

$$0 \le W_{P2G} \le W_{P2G,0} \tag{28}$$

where W_{P2G} represents the capacity of P2G; $\kappa_{P2G,g}^{down}$ and $\kappa_{P2G,g}^{up}$ represent the ramp-up and ramp-down limits of P2G, respectively; and $W_{P2G,0}$ represents the initial capacity of P2G.

6) Energy storage operation constraint

$$\begin{cases} 0 \le P_{i,c}(t) \le \gamma_{i,c} B_{i,c}(t) W_i \\ 0 \le P_{i,d}(t) \le \gamma_{i,d} B_{i,d}(t) W_i \\ \nu_{i,\min} W_i \le W_i(t) \le \nu_{i,\max} W_i \\ B_{i,c}(t) + B_{i,d}(t) \le 1 \\ W_i(0) = W_i(T) \end{cases} \tag{29}$$

$$0 \le W_i \le W_{i,0} \tag{30}$$

where $\gamma_{i,c}$ and $\gamma_{i,d}$ represent the maximum charging and discharging rates of energy storage equipment i, respectively; W_i represents the total capacity of energy storage equipment i; $B_{i,c}(t)$ and $B_{i,d}(t)$ are binary variables, which represent the charging and discharging state parameters of energy storage equipment i during time period t, respectively; $\nu_{i,\min}$ and $\nu_{i,\max}$ represent the minimum and maximum state of charge value of energy storage equipment i, respectively; and $W_{i,0}$ represents the initial total capacity of energy storage equipment i.

7) Electricity power purchase constraint

$$0 \le P_{E,buy}(t) \le P_{E,buy}^{\max} \tag{31}$$

where $P_{E,buy}^{\max}$ represents the maximum electricity power purchased from PG.

8) Gas power purchase constraint

$$0 \le P_{G,buy}(t) \le P_{G,buy}^{\max} \tag{32}$$

where $P_{G,buy}^{\max}$ represents the maximum gas power purchased from GG.

9) Electricity power balance constraint

$$P_{WT}(t) + P_{PV}(t) + P_{E,buy}(t) + P_{CHP,e}(t) + P_{EES,d}(t) = P_{P2G,e}(t) + P_{EES,c}(t) + P_{E,load}(t) \tag{33}$$

where $P_{EES,c}(t)$ and $P_{EES,d}(t)$ represent the charging and discharging power of EES during time period t, respectively; and $P_{E,load}(t)$ represents the electricity load demand on the user side during time period t.

10) Heat power balance constraint

$$P_{CHP,h}(t) + P_{GB,h}(t) + P_{HES,d}(t) = P_{HES,c}(t) + P_{H,load}(t) \tag{34}$$

where $P_{HES,c}(t)$ and $P_{HES,d}(t)$ represent the charging and discharging power of HES during time period t, respectively; and $P_{H,load}(t)$ represents the heat load demand on the user side during time period t.

11) Gas power balance constraint

$$P_{G,buy}(t) + P_{P2G,g}(t) + P_{GES,d}(t) = P_{CHP,g}(t) + P_{GB,g}(t) + P_{GES,c}(t) + P_{G,load}(t) \tag{35}$$

where $P_{GES,c}(t)$ and $P_{GES,d}(t)$ represent the charging and discharging power of GES during time period t, respectively; $P_{CHP,g}(t)$ represents the gas power consumption of CHP during time period t; $P_{GB,g}(t)$

represents the gas consumption power of GB during time period t; and $P_{G,load}(t)$ represents the gas load demand on the user side during time period t.

3.3. Solution method

The IES optimal operation model developed in this study belongs to the mixed integer nonlinear programming problem. The standard form of the problem can be formulated as [31]:

$$\min C(y) \quad s.t. \begin{cases} g_l(y) = 0 & l = 1,2,\cdots,m \\ h_l(y) \le 0 & l = 1,2,\cdots,n \\ u \cdot y_{\min} \le y \le u \cdot y_{\max} \\ u \in \{0,1\} \end{cases} \tag{36}$$

where $C(y)$ represents the objective function; $g_l(y)$ and $h_l(y)$ represent the equality and inequality constraints, corresponding to the power balance constraints and the equipment operation power constraints, respectively; m and n represent the number of equality and inequality constraints, respectively; $y_{\min}$ and $y_{\max}$ represent the upper and lower limits of the equipment operation power, respectively; and u represents the state variable.

For the aforementioned problem, this study transforms it into a mixed integer linear programming problem, which can be directly solved by CPLEX.

4. Source load uncertainty mechanism

When the probability distributions of uncertain parameters are unknown, the IGDT can be used to provide a more robust solution by maximizing the fluctuation intervals of uncertain parameters from their predicted values and actual values [32].

4.1. Modeling of the source load uncertainty problem

When the IGDT is used to solve uncertainty problems, it is necessary to model those uncertainties as functions of their predicted values, which can be expressed as:

$$\begin{cases} Y \in U(R, Y^{'}) \\ U(R, Y^{'}) = \left\{ Y : \left| Y - Y^{'} \right| \le RY^{'} \right\} \end{cases} \tag{37}$$

where $Y^{'}$ represents the predicted value of the uncertain parameter; R represents the fluctuation degree of the uncertain parameter; and $U(R,\ Y^{'})$ represents the fluctuation interval of the uncertain parameter, which is set within $[Y^{'}(1-R),\ Y^{'}(1+R)]$.

According to Eq (31), the uncertainties of WT, PV, and load demands are modeled as the functions of their predicted values, which can be expressed as:

$$\begin{cases} U(R_{WT}, P_{WT}^{'}(t)) = \left\{ P_{WT}(t) : \left| P_{WT}(t) - P_{WT}^{'}(t) \right| \le R_{WT} P_{WT}^{'}(t) \right\} \\ U(R_{PV}, P_{PV}^{'}(t)) = \left\{ P_{PV}(t) : \left| P_{PV}(t) - P_{PV}^{'}(t) \right| \le R_{PV} P_{PV}^{'}(t) \right\} \\ U(R_{E}, P_{E,load}^{'}(t)) = \left\{ P_{E,load}(t) : \left| P_{E,load}(t) - P_{E,load}^{'}(t) \right| \le R_{E} P_{E,load}^{'}(t) \right\} \\ U(R_{H}, P_{H,load}^{'}(t)) = \left\{ P_{H,load}(t) : \left| P_{H,load}(t) - P_{H,load}^{'}(t) \right| \le R_{H} P_{H,load}^{'}(t) \right\} \\ U(R_{G}, P_{G,load}^{'}(t)) = \left\{ P_{G,load}(t) : \left| P_{G,load}(t) - P_{G,load}^{'}(t) \right| \le R_{G} P_{G,load}^{'}(t) \right\} \\ R_{WT} \ge 0, R_{PV} \ge 0, R_{E} \ge 0, R_{H} \ge 0, R_{G} \ge 0 \end{cases} \tag{38}$$

where R_{WT}, R_{PV}, R_E, R_H, and R_G represent the fluctuation degrees of WT, PV, electricity load, heat load, and gas load, respectively; and $P_{WT}^{'}(t)$, $P_{PV}^{'}(t)$, $P_{E,load}^{'}(t)$, $P_{H,load}^{'}(t)$, and $P_{G,load}^{'}(t)$ represent the predicted values of WT, PV, electricity load, heat load, and gas load, respectively.

4.2. Operation model based on information gap decision theory

The IGDT solves the adverse effects of uncertainty problems by establishing a robust model with the risk-averse strategy. The risk-averse strategy aims to maximize the fluctuation degrees of uncertain parameters while ensuring that the TO cost does not exceed the expected operation target cost. The robustness of the system increases with the calculated value of R; however, the TO cost will increase at the same time. The risk-averse strategy can be expressed as:

$$\max R$$
$$s.t. \begin{cases} \max C \le (1+\mu_c) C_0 \\ \forall P_{WT}(t) \in U(R_{WT,} P_{WT}^{'}(t)) \\ \forall P_{PV}(t) \in U(R_{PV,} P_{PV}^{'}(t)) \\ \forall P_{E,load}(t) \in U(R_{E,} P_{E,load}^{'}(t)) \\ \forall P_{H,load}(t) \in U(R_{H,} P_{H,load}^{'}(t)) \\ \forall P_{G,load}(t) \in U(R_{G,} P_{G,load}^{'}(t)) \\ \text{Eqs. (19)} - \text{(35)} \end{cases} \tag{39}$$

where C_0 is the optimal TO cost when the uncertain parameters are equal to their predicted values; μ_c represents the risk-averse coefficient, with a larger value indicating a stronger risk resistance capability of the system; and $(1+\mu_c)C_0$ represents the expected operation target cost under the risk-averse strategy.

It is evident that Eq (39) represents a two-layer model, which aims to maximize the fluctuation degrees of uncertain parameters. When the uncertain parameters $P_{WT}(t)$, $P_{PV}(t)$, $P_{E,load}(t)$, $P_{H,load}(t)$, and $P_{G,load}(t)$ fluctuate within their interval $U(R_{WT}, P_{WT}^{'}(t))$, $U(R_{PV}, P_{PV}^{'}(t))$, $U(R_E, P_{E,load}^{'}(t))$, $U(R_H, P_{H,load}^{'}(t))$, and $U(R_G, P_{G,load}^{'}(t))$, respectively, the TO cost cannot exceed the expected operation target cost $(1 + \mu_c)C_0$. Therefore, when $P_{WT}(t)$, $P_{PV}(t)$, $P_{E,load}(t)$, $P_{H,load}(t)$, and $P_{G,load}(t)$ are equal to $(1 - R_{WT})P_{WT}^{'}(t)$, $(1 - R_{PV})P_{PV}^{'}(t)$, $(1 + R_E)P_{E,load}^{'}(t)$, $(1 + R_H)P_{H,load}^{'}(t)$, and $(1 + R_G)P_{G,load}^{'}(t)$, respectively, the corresponding TO cost is maximized.

The aforementioned two-layer model can be transformed into the following single-layer model:

$$\max R$$
$$s.t.\begin{cases} \max C \le (1+\mu_c)C_0 \\ P_{WT}(t) = (1-R_{WT})P'_{WT}(t) \\ P_{PV}(t) = (1-R_{PV})P'_{PV}(t) \\ P_{E,load}(t) = (1+R_E)P'_{E,load}(t) \\ P_{H,load}(t) = (1+R_H)P'_{H,load}(t) \\ P_{G,load}(t) = (1+R_G)P'_{G,load}(t) \\ \text{Eqs. } (19)-(35) \end{cases} \tag{40}$$

5. Experiments and analysis

5.1. Parameter setting

In the following experiments, the unit operation time period is set to 1 h, and the typically predicted output factors of the WT and PV system are shown in Figure 2(a) [30,33]. The typically predicted curves of electricity, heat, and gas loads are shown in Figure 2(b) [30]. The time-of-use electricity price and gas price are shown in Table 1 [34]. The detailed parameters of the evaluated IES are shown in Appendix [26,28–30,35–39]. The low-carbon economic operation of IES is achieved by optimizing the output of each equipment, as well as the EPP and GPP.

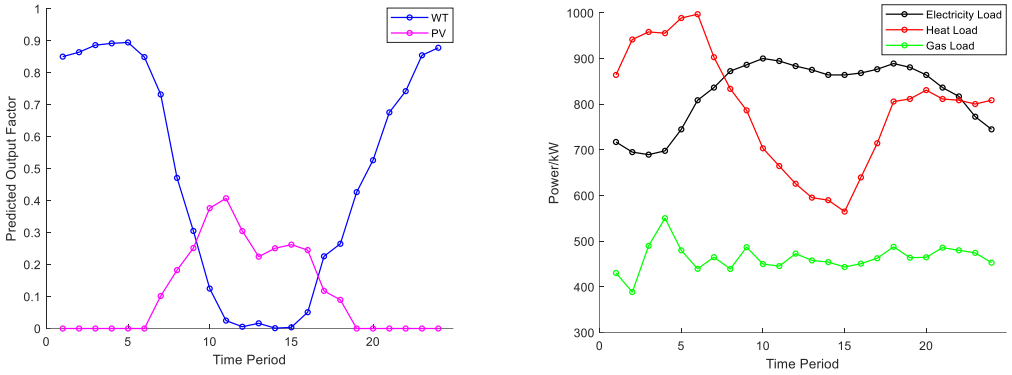

(a) Predicted output factors of WT and PV system

(b) Predicted curves of each energy load

Figure 2. Predicted output of renewable energy and multiple loads.

Table 1. Time-of-use electricity price and natural gas price.

Time period	Electricity price (CNY/(kW·h))	Gas price (CNY/(kW·h))
1–7, 23–24	0.48	0.35
8–11, 15–18	0.88	0.35
12–14, 19–22	1.10	0.35

To compare and verify the superiority of the method proposed in this study, the following five scenarios are set up for comparative analysis.

Scenario 1: Deterministic operation without considering IDR and EC optimization.

Scenario 2: Deterministic operation considering IDR but without EC optimization.

Scenario 3: Deterministic operation considering EC optimization but without IDR.

Scenario 4: Deterministic operation considering both IDR and EC optimization.

Scenario 5: IGDT robust operation considering the SLU problem, as well as IDR and EC optimization.

The operation results of the aforementioned scenarios are shown in Table 2. The detailed analysis will be presented in Sections 5.2 and 5.3.

Table 2. Operation results of the five scenarios.

Scenario	TO cost (CNY)	EPP cost (CNY)	GPP cost (CNY)	EM cost (CNY)	CT cost (CNY)	DEEI cost (CNY)	WPPAP cost (CNY)	CE (kg)
1	29130.69	2550.20	14525.07	5430.20	3442.43	3182.79	0	28788.92
2	27470.67	2479.09	14023.13	4943.33	2842.32	3182.79	0	25391.62
3	29042.47	2812.62	14420.63	5404.85	3373.74	3030.63	0	28656.26
4	27071.28	2859.40	13844.48	4905.74	2741.25	2720.41	0	25114.43
5	28424.85	3425.64	14477.08	4808.37	3109.75	2597.88	6.13	27560.31

5.2. Integrated demand response benefits analysis

5.2.1. Operational optimization analysis

The operational optimization of IES is solved by using the commercial solver CPLEX, in which the branch and bound algorithm played a critical role. The algorithm decomposes the original problem into multiple subproblems and then gradually eliminates branches that cannot achieve the optimal solution. Therefore, the optimal solution is found. Scenarios 1 and 2 are used to compare the impact of IDR on IES operation. As shown in Table 2, when IDR is considered in Scenario 2, all cost items are lower than those of Scenario 1. Specifically, the TO cost and CE are reduced by 5.70% and 11.80% respectively; thereby, the economic and environmental performance of IES is enhanced. The operation results of electricity, heat, and gas loads in Scenarios 1 and 2 are shown in Figures 3, 4, and 5 respectively.

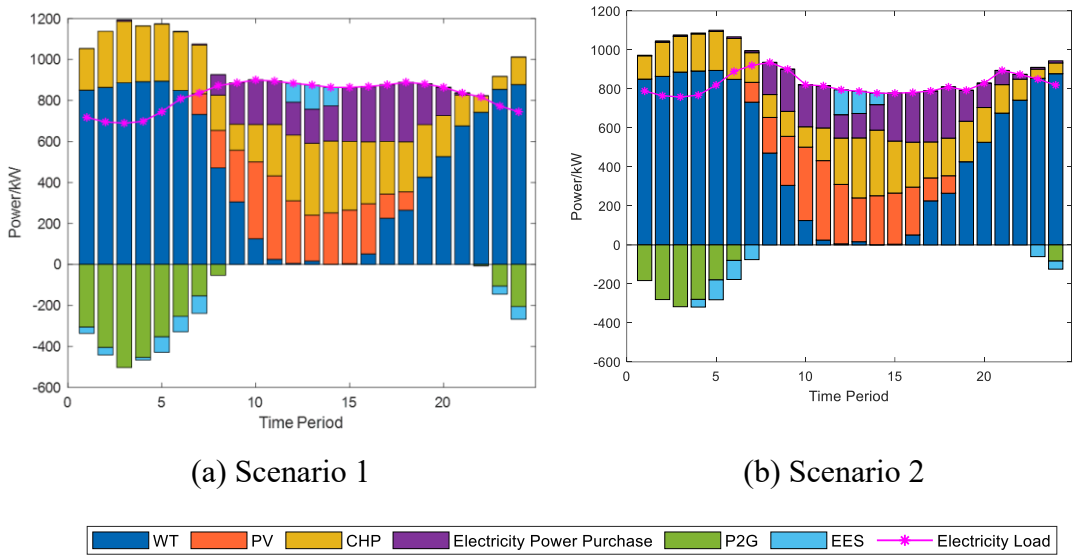

(a) Scenario 1 (b) Scenario 2

Figure 3. Electricity power balance diagrams in Scenarios 1 and 2.

Electricity power balance diagrams are plotted in Figure 3. It can be seen that in both Scenarios 1 and 2, the IES prioritizes the utilization of WT and PV power. In Scenario 2, when IDR is considered, the electricity load curve rises during the off-peak electricity price time periods 1–7 and 23–24. Since the CHP operating cost is higher than the EPP cost during these time periods, the IES reduces the use of CHP and P2G and increases the EPP from PG. Compared with Scenario 1, the total output of CHP is reduced from 2045.65 to 1329.79 kW (34.99% reduction), the total output of P2G is reduced from 2739.91 to 1401.73 kW (48.84% reduction), and the total EPP is increased from 17.89 to 64.63 kW (261.26% increase). As a result, the power stored in the EES is larger. In addition, during the time periods 8–22, the electricity load curve in Scenario 2 is lower. Since the CHP operating cost is lower than the EPP cost during these time periods, the use of CHP is increased compared with the off-peak electricity price time periods 1–7 and 23–24, and the power discharged in the EES is larger. As discussed above, the introduction of IDR can effectively improve the energy supply strategy and reduce the EPP cost.

Heat power balance diagrams are plotted in Figure 4. In both Scenarios 1 and 2, the IES prioritizes the utilization of GB for heat supply during the peak heating time periods 1–9 and 21–24, and the deficits are supplied by CHP and HES. In Scenario 2, when IDR is considered, the heat load curve is lower during the peak heating time periods, which leads to a significant decrease in CHP utilization. During the time periods 10–20, as shown in Figure 3, Scenario 2 reduces the electricity consumption, which results in a lower reliance on CHP. Compared to Scenario 1, the total output of CHP is reduced from 3265.23 to 2587.02 kW (20.77% reduction). During these time periods, the heat load demand is increased, and mainly supplied by GB; thereby, the economic performance is enhanced. The total output of GB is increased from 4638.46 to 5667.10 kW (22.18% increase). In conjunction with the actual CE model, the operating power of natural gas-fired equipment is reduced, which leads to a significant decrease in the total CE over the entire operation cycle, which is in line with the results listed in Table 2.

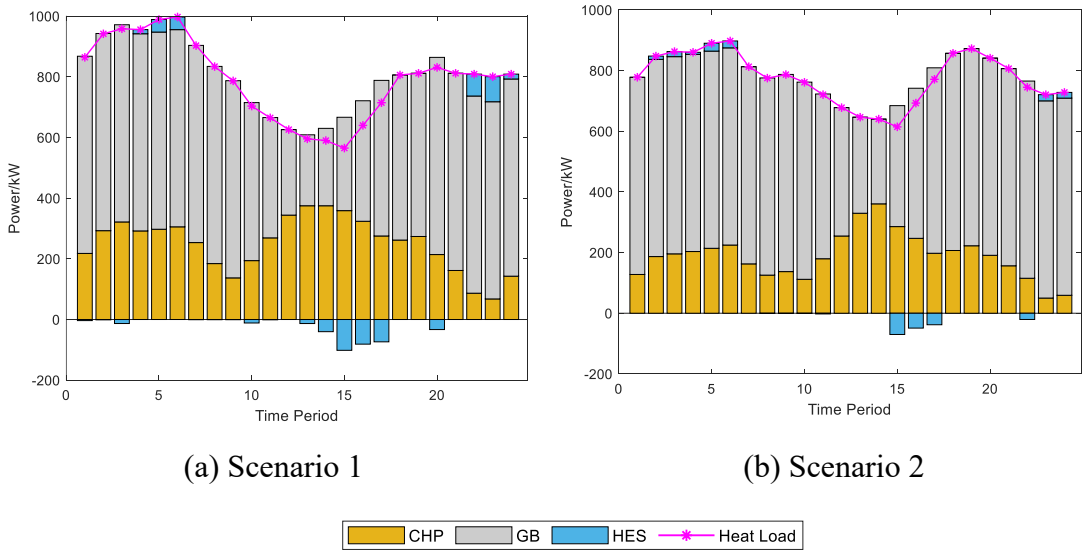

Figure 4. Heat power balance diagrams in Scenarios 1 and 2.

Gas power balance diagrams are plotted in Figure 5. During the off-peak electricity price time periods, the P2G is utilized by both Scenarios 1 and 2 to satisfy a portion of the gas load demand. At these time periods, the outputs of WT and PV are relatively high, and the presence of P2G enhances the consumption of renewable energy. During the peak and standard electricity price time periods, since the natural gas price remains constant and the operating cost of P2G is higher than the natural gas price, the required gas load is directly purchased from GG to improve economic performance. In Scenario 2, when IDR is considered, the gas load can be used to substitute for electricity and heat loads. Although the total amount of gas load is increased from 11122.77 to 11545.72 kW (3.80% increase) over the entire operation cycle, the natural gas price is lower, and the economic performance of Scenario 2 is still improved compared with Scenario 1.

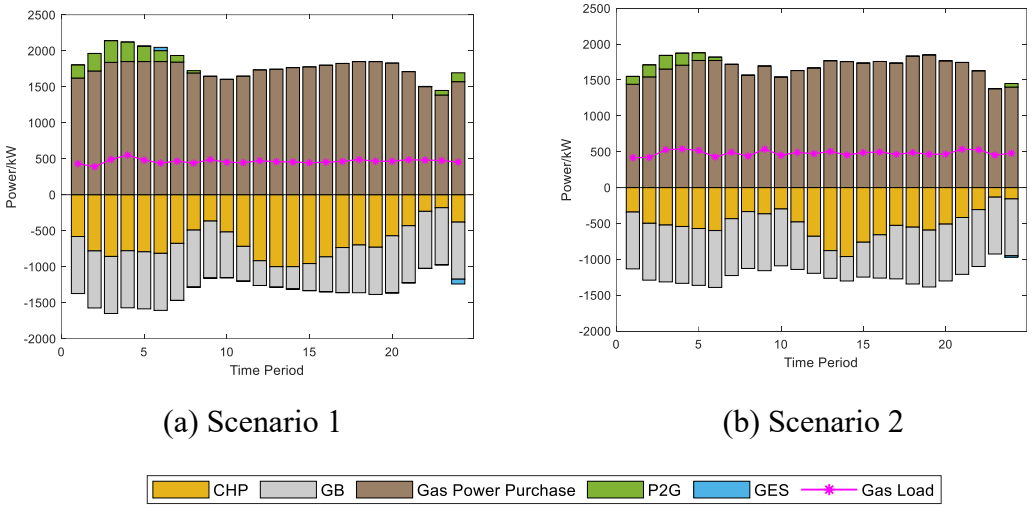

Figure 5. Gas power balance diagrams in Scenarios 1 and 2.

5.2.2. Load curve fluctuation analysis

In this section, Scenarios 1 and 2 are used to compare the impact of IDR on load fluctuation. The electricity, heat, and gas load curves in both Scenarios are plotted in Figure 6. It can be seen that the users consume less electricity and more heat during nighttime, and more electricity and less heat during the daytime. When IDR is considered, the load peak-to-valley differences are reduced according to the electricity price signal.

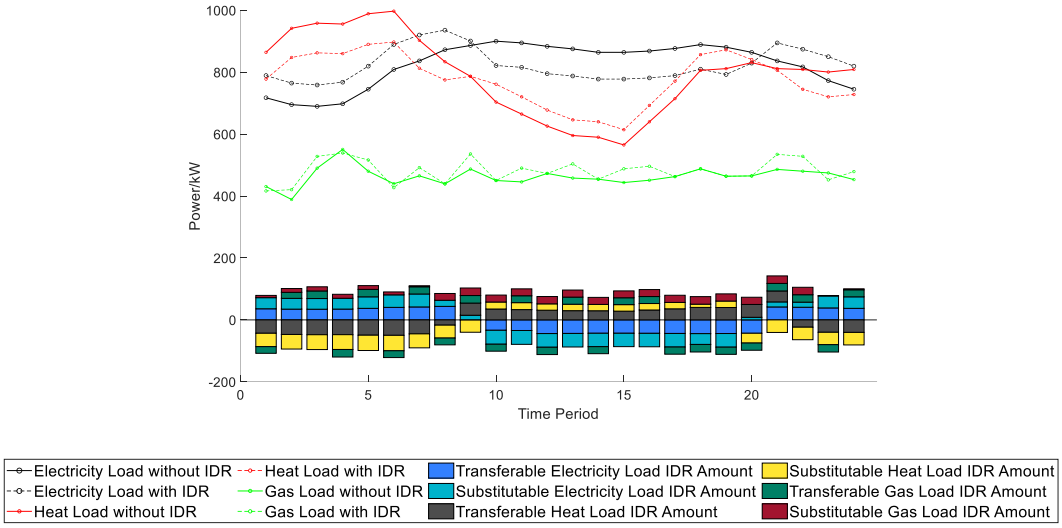

Figure 6. Load curves without and with IDR.

During time periods 1–9 and 21–24, in order to enhance the consumption of renewable energy, a lot of electricity load is transferred into these time periods, and some of the heat load is substituted by the electricity load. In addition, the heat load is high during the aforementioned time periods, which leads to a transfer of the heat load, and some of the heat load is substituted by the gas load. As a result, the electricity load curve and the heat load curve are relatively high and low during these time periods. During time periods 10–20, the users prefer to satisfy their energy demands with natural gas due to the higher electricity price, and some of the electricity load is substituted. Simultaneously, some of the electricity load is also substituted by the heat load, so the electricity load curve is decreased. According to the experimental results, the peak-to-valley differences of electricity, heat, and gas load curves are reduced by 32.02%, 34.48%, and 26.18% respectively. As discussed above, this optimization achieves the peak-cutting and valley-filling, significantly smooths the energy consumption curves, and reduces the power supply pressure of PG.

5.2.3. Equipment capacity optimization analysis

In Scenarios 3 and 4, the EC optimization is introduced into the IES operation control in order to further enhance the economic and environmental performance. As shown in Table 2, when Scenario 3 is compared with Scenario 1, and Scenario 4 is compared with Scenario 2, a significant reduction of TO cost and CE can be achieved when the EC optimization is introduced.

As shown in Table 2, when IDR is considered in Scenario 4, the DEEI cost is reduced by 10.24%.

Moreover, among all other cost items, only the electricity power purchase cost is slightly increased. In addition, the TO cost and CE in Scenario 4 are reduced by 6.79% and 12.36%, respectively. The results of EC optimization in Scenarios 3 and 4 are shown in detail in Figure 7.

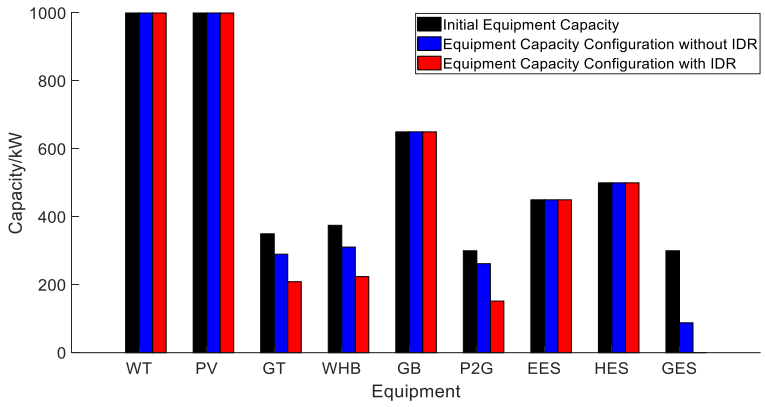

Figure 7. EC optimization results in Scenarios 3 and 4.

As shown in Figure 7, it can be seen that when the EC optimization is introduced in Scenarios 3 and 4, the capacities of GT, WHB, P2G, and GES are all reduced compared with the initial capacities, so the economic performance of IES operation is enhanced. This reduction stems from the fact that the previously oversized capacities are eliminated by exploiting temporal complementarity among WT, PV, and load profiles, which converts idle redundancy into tangible cost savings. In addition, when IDR is considered in Scenario 4, the capacities of GT, WHB, P2G, and GES are smaller, while the capacities of other equipment remain the same as in Scenario 3. Moreover, in Scenario 4, the GES capacity is 0, because the gas produced by P2G during the peak output periods of WT and PV can be consumed exactly, which makes the GES less useful for the operation of IES. Since the implementation of IDR can smooth the energy consumption curve and transfer the load from the peak time periods to the off-peak time periods, the power fluctuation of equipment output is decreased. Therefore, the capacities of partial equipment in Scenario 4 are smaller.

5.3. Source load uncertainty impact analysis

In Scenario 5, the IGDT based on the risk-averse robust model is introduced to solve the SLU problem, successfully obtaining the uncertain radii of WT, PV, electricity load, heat load, and gas load, which are $R_{WT} = 0.1023$, $R_{PV} = 0.0832$, $R_E = 0.0272$, $R_H = 0.0163$, and $R_G = 0.0109$, respectively. As shown in Table 2, the critical TO cost in Scenario 5 is 28,424.85 CNY, which indicates that when the actual values of WT, PV, electricity load, heat load, and gas load fluctuate within 10.23%, 8.32%, 2.72%, 1.63%, and 1.09% compared with the predicted values, the TO cost will not exceed 28,424.85 CNY. Scenarios 4 and 5 are used to compare the impact of the SLU problem on the operation of IES. The obtained power changes of certain equipment and EC optimization results are shown in Figure 8(a) and (b), respectively.

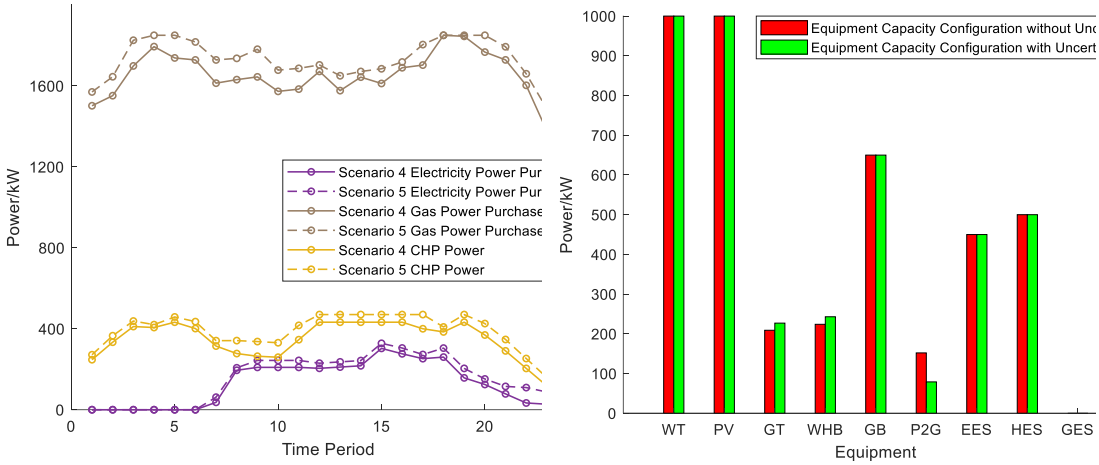

(a) Power changes of certain equipment in Scenarios 4 and 5

(b) EC optimization results in Scenarios 4 and 5

Figure 8. EC optimization and power changes results in Scenarios 4 and 5.

As shown in Figure 8(a,b), it can be seen that when the SLU problem is considered in Scenario 5, the IES adopts a more conservative output strategy to avoid the uncertainties. This strategy is achieved by increasing electricity power purchased from the PG and gas power purchased from the GG, while relying more on the stable output of CHP. Therefore, the capacity of P2G is reduced, while that of CHP is increased. This is in line with the results listed in Table 2, which shows that Scenario 5 experiences a 19.80% increase in EPP cost, a 4.57% increase in GPP cost, and a 9.74% increase in CE. As a result, although the TO cost is increased, the adjustability and risk-bearing ability of IES are significantly enhanced.

5.4. Different risk-averse coefficients impact analysis

Based on Scenario 5, the impact of different risk-averse coefficients on IES is deeply explored. The economic performance and uncertainty radii of loads are shown in Figure 9.

As shown in Figure 9, it can be seen that with the risk-aversion coefficients are increased, although the TO cost is higher, the uncertainty radii of loads are larger. For example, when the risk-aversion coefficients are increased from 0.05 to 0.20, the uncertainty radii of WT, PV, electricity load, heat load, and gas load are increased by 0.0966, 0.1014, 0.0896, 0.0538, and 0.0358, respectively. Therefore, the risk-resistance capability of IES is improved, which in turn makes its operation more stable.

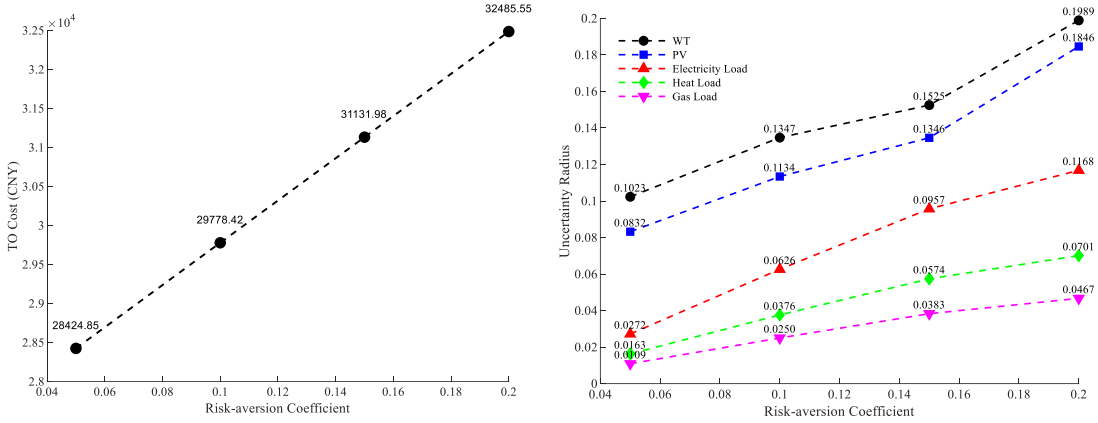

(a) Impact of risk-averse coefficients on TO cost

(b) Impact of risk-averse coefficients on uncertainty radii

Figure 9. Impact of risk-averse coefficients on TO cost and uncertainty radii.

6. Conclusions

In this study, an operation method that considers source load uncertainty and equipment capacity optimization is developed to achieve optimal operation of the integrated energy system. First, the system model, including electricity, heat, and gas loads, is established, in which the ladder-type carbon trading mechanism is introduced. Moreover, the integrated demand response (IDR) model is proposed by considering the horizontal transfer and vertical complementary substitution of loads. Second, the equipment capacity optimization of the system is introduced to minimize the comprehensive cost. Then, the optimal operation model is established, which is solved by the commercial solver CPLEX. Finally, the information gap decision theory is further introduced to solve the source load uncertainty problem, and a risk-averse robust model is also developed.

Experimental results show that when IDR is considered, the total operating cost and carbon emissions are reduced by 5.70% and 11.80%, respectively. Simultaneously, the peak-to-valley differences of electricity, heat, and gas load curves are reduced by 32.02%, 34.48%, and 26.18%, respectively, which achieves peak cutting and valley filling. In addition, when the equipment capacity optimization is further considered, the capacities of combined heating and power (CHP) and power-to-gas are reduced by 40.28% and 49.33%, respectively, and the capacity of gas energy storage is 0, in which the total operating cost and carbon emission are further reduced by 1.45% and 1.09%, respectively. Moreover, when the source load uncertainty is further considered, the system needs to purchase more electricity and gas to cope, while also tending to use the more stable CHP equipment. Therefore, although the total operation cost, carbon emissions, and capacity of CHP are increased by 5.00%, 9.74%, and 8.55%, respectively, the risk-bearing ability of the system is significantly improved. As discussed above, when source load uncertainty and equipment capacity optimization are considered, the economic and environmental performance of the system can be improved, while the operational stability is also ensured.

This study has many limitations. In the future, more efforts will be made to further improve the model accuracy of IES. The systematic multi-scenario sensitivity analysis should be conducted to

further examine the impacts of key parameters, such as the risk-averse coefficient of extreme weather events and the base price of carbon trading, on the optimal operation and carbon emission reduction effect.

Use of AI tools declaration

The authors declare that no Artificial Intelligence (AI) tools have been used in the creation or revision of this article. The content is entirely the original work of the authors.

Acknowledgments (All sources of funding of the study must be disclosed.)

This work is supported by the National Natural Science Foundation of China (Grant No. 52371334); the Hubei Natural Science Foundation Innovation and Development Joint Fund (Grant No. 2024AFD213).

Conflict of interest

The authors declare no conflicts of interest.

Author contributions

Conceptualization, Ruoli Tang and Xin Li; methodology, Ruoli Tang and Xin Li; software, Chao Jiang; validation, Yinchen Zhang and Xin Li; formal analysis, Xin Li; investigation, Zelong Li; resources, Chao Jiang; data curation, Chao Jiang; writing—original draft preparation, Ruoli Tang and Chao Jiang; writing—review and editing, Xin Li; visualization, Yinchen Zhang and Chao Jiang; supervision, Mingyue Xu; funding acquisition, Ruoli Tang. All authors have read and agreed to the published version of the manuscript.

References

1. Jia Y, Wan C, Cui W, et al. (2022) Peer-to-peer energy trading using prediction intervals of renewable energy generation. *IEEE Trans Smart Grid* 14: 1454–1465. https://doi.org/10.1109/TSG.2022.3168150
2. Woon KS, Phuang ZX, Taler J, et al. (2023) Recent advances in urban green energy development towards carbon emissions neutrality. *Energy* 267: 126502. https://doi.org/10.1016/j.energy.2022.126502
3. Chen X, Wang C, Wu Q, et al. (2020) Optimal operation of integrated energy system considering dynamic heat-gas characteristics and uncertain wind power. *Energy* 198: 117270. https://doi.org/10.1016/j.energy.2020.117270
4. Ma H, Chen Q, Hu B, et al. (2021) A compact model to coordinate flexibility and efficiency for decomposed scheduling of integrated energy system. *Appl Energy* 285: 116474. https://doi.org/10.1016/j.apenergy.2021.116474

5. Zhang G, Wang W, Chen Z, et al. (2022) Modeling and optimal dispatch of a carbon-cycle integrated energy system for low-carbon and economic operation. *Energy* 240: 122795. https://doi.org/10.1016/j.energy.2021.122795
6. Dong H, Fu Y, Jia Q, et al. (2022) Optimal dispatch of integrated energy microgrid considering hybrid structured electric-thermal energy storage. *Renewable Energy* 199: 628–639. https://doi.org/10.1016/j.renene.2022.09.027
7. Zhang D, Zhu H, Zhang H, et al. (2021) Multi-objective optimization for smart integrated energy system considering demand responses and dynamic prices. *IEEE Trans Smart Grid* 13: 1100–1112. https://doi.org/10.1109/TSG.2021.3128547
8. Ding YR, Chen HK, Wu J, et al. (2021) Multi-objective optimal dispatch of electricity-gas-heat integrated energy system considering comprehensive energy efficiency. *Autom Electric Power Syst* 45: 64–73. https://doi.org/10.7500/AEPS20200811002
9. Wang Y, Ma Y, Song F, et al. (2020) Economic and efficient multi-objective operation optimization of integrated energy system considering electro-thermal demand response. *Energy* 205: 118022. https://doi.org/10.1016/j.energy.2020.118022
10. Xiang Y, Cai H, Gu C, et al. (2020) Cost-benefit analysis of integrated energy system planning considering demand response. *Energy* 192: 116632. https://doi.org/10.1016/j.energy.2019.116632
11. Yang X, Chen Z, Huang X, et al. (2021) Robust capacity optimization methods for integrated energy systems considering demand response and thermal comfort. *Energy* 221: 119727. https://doi.org/10.1016/j.energy.2020.119727
12. Zhou L, Song A, Zhou Y (2024). Electrification and hydrogenation on a PV-battery-hydrogen energy flexible community for carbon-neutral transformation with transient aging and collaboration operation. *Energy Convers Manage* 300: 117984. https://doi.org/10.1016/j.enconman.2023.117984
13. Zhang X, Zhou Y (2024) Waste-to-energy (W2E) for renewable-battery-FCEV-building multi-energy systems with combined thermal/power, absorption chiller and demand-side flexibility in subtropical climates. *Energy Build* 307: 113949. https://doi.org/10.1016/j.enbuild.2024.113949
14. Yang M, Liu Y (2023) Research on multi-energy collaborative operation optimization of integrated energy system considering carbon trading and demand response. *Energy* 283: 129117. https://doi.org/10.1016/j.energy.2023.129117
15. Liu C, Fan Y, Yu W, et al. (2024) Low carbon operation and evaluation methods for integrated energy system counting EVs with whole life cycle considering demand response. *Renewable Energy* 236: 121447. https://doi.org/10.1016/j.renene.2024.121447
16. Li P, Cai YQ, Han XQ, et al. (2020) Optimization operation of AC/DC hybrid microgrid considering random fuzzy double uncertainties. *High Voltage Eng* 46: 2269–2279. https://doi.org/10.13336/j.1003-6520.hve.20200619001
17. Mei F, Zhang J, Lu J, et al. (2021) Stochastic optimal operation model for a distributed integrated energy system based on multiple-scenario simulations. *Energy* 219: 119629. https://doi.org/10.1016/j.energy.2020.119629
18. Sun K, Zhang QM, Wang L, et al. (2020) Two-stage robust planning for microgrid considering security margin. *Power Syst Technol* 44: 4617–4626. https://doi.org/10.13335/j.1000-3673.pst.2020.0292a

19. Ye HL, Liu S, Hu J, et al. (2021) Multi-source joint dispatching strategy for a power system with concentrating solar power plants based on IGDT. *Power Syst Prot Control* 49: 35–43. https://doi.org/10.19783/j.cnki.pspc.202114
20. Sun Q, Fu Y, Lin H, et al. (2022) A novel integrated stochastic programming-information gap decision theory (IGDT) approach for optimization of integrated energy systems (IESs) with multiple uncertainties. *Appl Energy* 314: 119002. https://doi.org/10.1016/j.apenergy.2022.119002
21. Wang L, Dong H, Lin J, et al. (2022) Multi-objective optimal scheduling model with IGDT method of integrated energy system considering ladder-type carbon trading mechanism. *Int J Electr Power Energy Syst* 143: 108386. https://doi.org/10.1016/j.ijepes.2022.108386
22. Jordehi AR, Javadi MS, Shafie-khah M, et al. (2021) Information gap decision theory (IGDT)-based robust scheduling of combined cooling, heat and power energy hubs. *Energy* 231: 120918. https://doi.org/10.1016/j.energy.2021.120918
23. Peng CH, Chen L, Zhang JK, et al. (2020) Multi-objective optimal allocation of energy storage in distribution network based on classified probability chance constraint information gap decision theory. *Proc CSEE* 40: 2809–2819. https://doi.org/10.13334/j.0258-8013.pcsee.190551
24. Zhang DH, Yun YY, Wang XJ, et al. (2021) Economic dispatch of integrated electricity-heat-gas energy system considering generalized energy storage and concentrating solar power plant. *Autom Electr Power Syst* 45: 33–42. https://doi.org/10.7500/AEPS20210220002
25. Pan H, Yao Z, Lin SF, et al. (2022) Low-carbon dispatch optimization of integrated energy system including solar power plant and heat pump based on information gap decision theory. *Mod Electr Power* 39: 169–183. https://doi.org/10.19725/j.cnki.1007-2322.2021.0058
26. Yuan SQ, Pan PC, Wei YW, et al. (2024) Study on low-carbon economic optimal scheduling model of community integrated energy system. *Acta Energiae Solaris Sinica* 45: 347–356. https://doi.org/10.19912/j.0254-0096.tynxb.2022-1784
27. Guo Y, Wang D, Li SY, et al. (2022) Optimal allocation of energy storage in regional integrated energy system based on security region. *Power Syst Technol* 46: 604–614. https://doi.org/10.13335/j.1000-3673.pst.2021.0474
28. Qin T, Liu HD, Wang JQ, et al. (2018) Carbon trading based low-carbon economic dispatch for integrated electricity-heat-gas energy system. *Autom Electr Power Syst* 42: 8–13. https://link.cnki.net/urlid/32.1180.TP.20180605.1054.006
29. Yang HH, Xie MY, Huang WT, et al. (2021) Low-carbon economic operation of urban integrated energy system including waste treatment. *Power Syst Technol* 45: 3545–3552. https://doi.org/10.13335/j.1000-3673.pst.2020.1676
30. Chen JP, Hu ZJ, Chen JB, et al. (2021) Optimal dispatch of integrated energy system considering ladder-type carbon trading and flexible double response of supply and demand. *High Voltage Eng*, 47: 3094–3106. https://doi.org/10.13336/j.1003-6520.hve.20211094
31. Yang HZ, Li ML, Jiang ZY, et al. (2020) Optimal operation of regional integrated energy system considering demand side electricity heat and natural-gas loads response. *Power Syst Prot Control* 48: 30–37. https://doi.org/10.19783/j.cnki.pspc.190774
32. Wang CQ, Wei H, Wu SY, et al. (2018) Multi-power combined unit commitment based on information gap decision theory. *Proc CSEE* 38: 3431–3440. https://doi.org/10.13334/j.0258-8013.pcsee.171096

33. Feng ZY, Xu YX, Wang KL, et al. (2024) Optimal configuration of battery energy storage capacity of microgrid considering life loss. *J Power Supply* 22: 101–109. https://doi.org/10.13234/j.issn.2095-2805.2024.1.101
34. Li P, Wang ZX, Hou L, et al. (2019) Analysis of repeated game based optimal operation for regional integrated energy system. *Autom Electr Power Syst* 43: 81–89. https://doi.org/10.7500/AEPS20181115007
35. Wang K, Li Y, Yu JC, et al. (2024) Double layer optimization model for capacity configuration and operation strategy of electric-thermal integrated energy system. *Distrib Util* 41: 55–63. https://doi.org/10.19421/j.cnki.1006-6357.2024.06.007
36. Wang S, Sun X, Xie JD, et al. (2023) Optimization of double-layer capacity configuration for comprehensive energy systems considering supply reliability. *Mod Electr Power* 40: 1–14. https://doi.org/10.19725/j.cnki.1007-2322.2023.0128
37. Hou JM, Ding SY, Yu WJ, et al. (2023) Capacity allocation of integrated energy system involving multiple investors. *J Naning Univ Inf Sci Technol* 15: 703–711. https://doi.org/10.13878/j.cnki.jnuist.20220223001
38. Lu BW, Wei ZB, Wei PA, et al. (2021) Optimal configuration of PtG and energy storage equipment in regional integrated energy system considering wind power consumption. *Smart Power* 49: 7–14. https://doi.org/10.3969/j.issn.1673-7598.2021.05.003
39. Men XY, Cao J, Wang ZS, et al. (2018) The constructing of multi-energy complementary system of energy internet microgrid and energy storage model analysis. *Proc CSEE* 38: 5727–5737. https://doi.org/10.13334/j.0258-8013.pcsee.172419

Appendix

Detailed parameter settings.

Parameter	Value	Parameter	Value	Parameter	Value
$\eta_{P2G,g}$	0.60	$\eta_{GT,e}$	0.35	$\eta_{GT,loss}$	0.15
$\eta_{WHB,h}$	0.75	L_{NG}	9.7 kW·h /m³	$\eta_{GB,h}$	0.82
σ_{EES}	0.01	σ_{HES}	0.01	σ_{GES}	0.01
$\eta_{EES,c}$	0.90	$\eta_{HES,c}$	0.90	$\eta_{GES,c}$	0.90
$\eta_{EES,d}$	0.90	$\eta_{HES,d}$	0.90	$\eta_{GES,d}$	0.90
α_E	0.798 kg/(kW·h)	α_H	0.385 kg/(kW·h)	$\alpha_{E,h}$	6 MJ/(kW·h)
$\alpha_{G,load}$	0.180 kg/(kW·h)	T	24 h	x_1	35
y_1	−0.38	z_1	0.0034	x_2	3
y_2	−0.004	z_2	0.001	β	0.20 kg/(kW·h)
γ	0.69 kg/(kW·h)	λ	0.252 CNY/kg	d	2000kg
δ	0.25	$\varepsilon^t_{K,\min}$	−0.05	$\varepsilon^t_{K,\max}$	0.05
$\varepsilon^s_{K,\min}$	−0.05	$\varepsilon^s_{K,\max}$	0.05	$C_{M,WT}$	0.08 CNY/kW
$C_{M,PV}$	0.11 CNY/kW	$C_{M,GT}$	0.15 CNY/kW	$C_{M,WHB}$	0.15 CNY/kW
$C_{M,GB}$	0.15 CNY/kW	$C_{M,P2G}$	0.20 CNY/kW	$C_{M,EES}$	0.10 CNY/kW
$C_{M,HES}$	0.10 CNY/kW	$C_{M,GES}$	0.10 CNY/kW	C_{WT}	4800 CNY/kW

Continued on next page

Parameter	Value	Parameter	Value	Parameter	Value
C_{PV}	4000 CNY/kW	C_{GT}	4000 CNY/kW	C_{WHB}	1000 CNY/kW
C_{GB}	500 CNY/kW	C_{P2G}	8000 CNY/kW	C_{EES}	600 CNY/kW
C_{HES}	50 CNY/kW	C_{GES}	130 CNY/kW	N_{WT}	20 Year
N_{PV}	25 Year	N_{GT}	20 Year	N_{WHB}	20 Year
N_{GB}	18 Year	N_{P2G}	20 Year	N_{EES}	10 Year
N_{HES}	10 Year	N_{GES}	20 Year	r	0.06
χ_{DG}	0.1 CNY/(kW·h)	$\kappa_{CHP,e}^{down}$	−0.20	$\kappa_{CHP,e}^{up}$	0.20
$\kappa_{GB,h}^{down}$	−0.20	$\kappa_{GB,h}^{up}$	0.20	$\kappa_{P2G,}^{down}$	−0.20
$\kappa_{P2G,g}^{up}$	0.20	$\gamma_{EES,c}$	0.50	$\gamma_{EES,d}$	0.50
$\gamma_{HES,c}$	0.50	$\gamma_{HES,d}$	0.50	$\gamma_{GES,c}$	0.50
$\gamma_{GES,d}$	0.50	$v_{EES,\min}$	0.1	$v_{EES,\max}$	0.9
$v_{HES,\min}$	0.1	$v_{HES,\max}$	0.9	$v_{GES,\min}$	0.1
$v_{GES,\max}$	0.9	$P_{E,buy}^{\max}$	1850 kW	$P_{G,buy}^{\max}$	1850 kW
$W_{WT,0}$	1000 kW	$W_{PV,0}$	1000 kW	$W_{GT,0}$	350 kW
$W_{WHB,0}$	375 kW	$W_{GB,0}$	650 kW	$W_{P2G,0}$	300 kW
$W_{EES,0}$	450 kW	$W_{HES,0}$	500 kW	$W_{GES,0}$	300 kW
$W_{EES}(0)$	135 kW	$W_{HES}(0)$	150 kW	$W_{GES}(0)$	90 kW
μ_c	0.05	——	——	——	——